Carbohydrate Polymers 83 (2011) 239–245

Contents lists available at ScienceDirect

Carbohydrate Polymers

journal homepage: www.elsevier.com/locate/carbpol

Enhanced bacterial inhibition activity of layer-by-layer structured polysaccharide film-coated cellulose nanofibrous mats via addition of layered silicate

Hongbing Deng[a,b,1], Xiaoying Wang[c,1], Pu Liu[d], Bin Ding[b,e,*], Yumin Du[a,**], Guoxiang Li[a], Xianwen Hu[a], Jianhong Yang[a]

[a] School of Resource and Environmental Science, Wuhan University, Wuhan 430079, China
[b] State Key Laboratory for Modification of Chemical Fibers and Polymer Materials, Donghua University, Shanghai 201620, China
[c] State Key Laboratory of Pulp and Paper Engineering, School of Light Industry and Food, South China University of Technology, Guangzhou 510640, China
[d] National Center of Citrus Breeding, Key Laboratory of Horticultural Plant Biology of Ministry of Education, Huazhong Agricultural University, Wuhan 430070, China
[e] Nanomaterials Research Center, Modern Textile Institute, Donghua University, Shanghai 200051, China

ARTICLE INFO

Article history:
Received 24 June 2010
Received in revised form 20 July 2010
Accepted 21 July 2010
Available online 30 July 2010

Keywords:
LBL
Electrospinning
Polysaccharide
Organic rectorite
Intercalation
Bacterial inhibition activity

ABSTRACT

Organic rectorite (OREC) was used to prepare the intercalated composites with chitosan (CS). The negatively charged cellulose nanofibers hydrolyzed from electrospun cellulose acetate fibrous mats were modified with multilayers of the positively charged CS-OREC intercalated composite and the negatively charged sodium alginate (ALG) via layer-by-layer (LBL) technique. The morphology and antibacterial activity of the resultant samples were studied by regulating the number of deposition bilayers, the compositions of dipping solutions and outermost layer of films. Field emission scanning electron microscopy images indicated that the thickness of CS-OREC/ALG bilayer formed on fibers was estimated from 12 to 26 nm. Additionally, the energy-dispersive X-ray spectroscopy and X-ray photoelectron spectroscopy results indicated that CS and OREC were successfully deposited on cellulose fibers. The bacterial inhibition experiments demonstrated that LBL films modified fibrous cellulose mats with the addition of OREC can increase the degree of inhibition on *Escherichia coli*.

1. Introduction

Electrostatic layer-by-layer (LBL) self-assembly technique, introduced by Decher and Hong (1991), is a powerful and efficient method to form multilayer ultra-thin films (Decher, 1997; Xiao et al., 2009) on selected substrates with various shapes and sizes (Elbakry et al., 2009; Kim et al., 2007; Zhang, Chen, Sun, & Shen, 2007). Recently, nanofibrous mats obtained via electrospinning were used as templates for LBL deposition because of their unique characteristics such as ultra-thin fiber diameter, small pore size, high specific surface, three-dimensional (3D) structure, etc. (Ding, Kimura, Sato, Fujita, & Shiratori, 2004; Ding, Li, Miyauchi, Kuwaki, & Shiratori, 2006; Ji et al., 2006; Lee, Kim, Chen, Shao-Horn, & Hammond, 2009; Yang, Tao, Pang, & Siu, 2008). The fibrous mats with negatively or positively charged fiber surface, low fiber density, and good water insolubility can be regarded as ideal templates for LBL deposition (Ding, Li, Fujita, & Shiratori, 2006).

By using the LBL self-assembly technique, various deposition materials have been used to fabricate the functional LBL structured composite films including polymers, metal irons, particles, etc. (Ding, Li, Fujita et al., 2006; Srivastava & Kotov, 2008; Unal et al., 2006; Wang, Shi, Chen, & Baker, 2009). Composite materials could be more effective and attractive than single material. Nowadays, polymer/layered silicate composites attracted intensive attentions because they possess properties of both organic and inorganic materials (Darder, Colilla, & Ruiz-Hitzky, 2003; Giannelis, Krishnamoorti, & Manias, 1999; Wang et al., 2006). Polymer/layered silicate composites could be good candidates as deposition materials to form LBL structured films to improve the properties of the templates. Our previous studies found that rectorite (REC), especially organic rectorite (OREC, modified from REC), may be more preferred because of their larger interlayer distance, better separable layer thickness and layer aspect ratio compared with regular layered silicates such as montmorillonite (Wang et al., 2006; Wang, Du et al., 2009; Wang, Pei, Du, & Li, 2008; Wang, Strand, Du, & Varum, 2010). Moreover, N-(2-hydroxyl) propyl-3-trimethyl ammonium chitosan (CS) chloride-OREC intercalated composite was proved to be positively charged when it is dispersed in an aqueous solution system (Wang, Du et al., 2009), so it would be hypothesized that CS-OREC composite was positively charged and suitable as a novel deposition materials for LBL deposition.

* Corresponding author at: State Key Laboratory for Modification of Chemical Fibers and Polymer Materials, Donghua University, Shanghai 201620, China. Tel.: +86 21 62378202; fax: +86 21 62378392.
** Corresponding author. Tel.: +86 27 68778501; fax: +86 27 68778501.
E-mail addresses: binding@dhu.edu.cn (B. Ding), duyumin@whu.edu.cn (Y. Du).
[1] Co-first author with the same contribution to this work.

0144-8617/$ – see front matter © 2010 Elsevier Ltd. All rights reserved.
doi:10.1016/j.carbpol.2010.07.042

CS, the second most abundant cationic polysaccharide in nature, is useful in many different applications, one of which is as a natural antimicrobial agent. CS has more advantages than other types of disinfectants because of its higher antibacterial activity, broader spectrum of activity, higher killing rate and lower toxicity towards mammalian cells (Shahidi, Arachchi, & Jeon, 1999; Wang, Du et al., 2009). In order to further improve its antibacterial ability, the complexes of CS and other additives were prepared. The complexes have good bacteriostatic activity, strong immobilization of bacterial and inhibition of bacterial proliferation. Recently, Wang et al. reported that the intercalated CS-OREC composites have better antibacterial activity than CS itself because OREC could adsorb more bacterial and inhibit its proliferation (Wang et al., 2006).

Encouraged by our previous success in the formation of intercalated CS-OREC composites (Wang et al., 2006), we developed a straightforward and highly efficient method to fabricate polysaccharide-OREC intercalation deposited nanofibrous cellulose mats with bacterial inhibition activity via LBL self-assembly, which may expand the applications of nanofibrous cellulose mats.

The current research focused on generating novel LBL films on nanofibrous polysaccharide template, specifically cellulose nanofibers hydrolyzed from electrospun cellulose acetate nanofibers (Liu & Hsieh, 2002). Intercalated CS-OREC composite and sodium alginate (ALG, a kind of anionic polysaccharide) were selected as deposition materials to be coated on cellulose nanofibers via electrostatic LBL self-assembly technique by alternative adsorption of positively charged intercalated CS-OREC composite and negatively charged ALG in aqueous media. The effect of the outermost layer variation, the number of deposition bilayers, and the composition of the multilayer on the formation of the LBL structured nanofibrous mats was investigated. Meanwhile, the bacterial inhibition experiments were performed to determine the antimicrobial property of the resultant samples.

2. Experimental details

2.1. Materials

The starting materials included cellulose acetate (CA, M_n 3×10^4, Aldrich Co., USA), chitosan (CS, M_w 2.1×10^5 kDa, DD 92%, Yuhuan Ocean Biochemical Co., China), calcium rectorite (REC, Mingliu Inc. Co., China), sodium alginate (ALG, M_w 2.5×10^5 kDa, Aladdin Chemical Plant, China). All aqueous solutions were prepared using purified water with a resistance of 18.2 MΩ cm. In addition, the organic rectorite (OREC) and the intercalated CS-OREC were prepared according to our previous report (Wang et al., 2006). Briefly, the REC was dispersed in purified water to obtain the clay suspension under vigorous stirring for 30 min, and then left standing for 24 h. Sodium dodecylsulfonate (SDS) solution was added slowly into the above suspension at 90 °C with 5 h stirring. The resultant product was washed several times with purified water and filtered to remove excessive SDS. The sample was dried at 90 °C to yield OREC. Additionally, CS was dissolved in 0.002 M aqueous acetic acid and then added slowly into the pretreated OREC suspension with stirring at 60 °C for 2 days to obtain the composites with initial CS:OREC weight ratio of 12:1. The resulting mixture was then precipitated with 1 M NaOH. The formed composites were washed with distilled water until the solution became neutral. Finally the CS-OREC composites were dried at 50 °C and grounded to powder.

2.2. Electrospinning of CA nanofibrous mats and their hydrolysis

Nanofibrous CA mats were fabricated from 15 wt% CA solution prepared with 2/1 (w/w) acetone/N,N-dimethylacetamide mixture solvent. The CA solution was placed in a plastic syringe which connected to a metal needle tip. The syringe was driven by a syringe pump (LSP02-1B, Baoding Longer Precision Pump Co., Ltd., China). The positive electrode of a high voltage power supply (DW-P303-1ACD8, Tianjin Dongwen High Voltage Co., China) was clamped to the tip of the syringe. A grounded cylindrical collector covered by aluminum foil was rotated with a linear velocity of 100 m/min. The applied voltage was 16 kV, and the tip-to-collector distance was 20 cm. The ambient temperature and relative humidity were maintained at 25 °C and 40%, respectively. Then the prepared fibrous mats were dried at 80 °C to remove trace solvents under vacuum. Hydrolysis of the CA mats was performed in a 0.05 M NaOH aqueous solution at room temperature for 7 days following the previously reported procedure (Ingrosso et al., 2006).

2.3. Preparation of dipping solutions for LBL process

The concentration of the positively charged CS and CS-OREC (12/1, w/w) solutions was fixed as 1 mg/mL by dissolving them in a 0.002 M aqueous acetic acid solution and the pH of solutions was controlled at 5. The negatively charged ALG solution was 1 mg/mL in pure water and the pH was adjusted to 4. The ionic strength of all dipping solutions was regulated by the addition of NaCl at a concentration of 0.1 M.

2.4. Formation of LBL structured multilayer on nanofibrous mats

First, nanofibrous cellulose mats were immersed into CS or intercalated CS-OREC suspensions for 20 min followed by 2 min of rinsing in three pure water baths (Deng et al., 2010). The mats were then immersed into the ALG solution for 20 min, followed by the identical rinsing steps. The adsorption and rinsing steps were repeated until the desired number of deposition bilayers was obtained. Here, $(CS\text{-}OREC/ALG)_n$ was used as a formula to label the LBL structured films, where n was the number of the CS-OREC/ALG bilayers. The outermost layer was CS-OREC composite when n equaled to 5.5 and 10.5. The LBL films coated fibrous mats were dried at 80 °C for 24 h under vacuum prior to further characterizations.

2.5. Characterization

The morphology and composition of fibrous mats were examined by field emission scanning electron microscopy (FE-SEM) and energy-dispersive X-ray (EDX) spectroscopy (S-4800, Hitachi Ltd., Japan). The diameters of the fibers were measured using image analyzer (Adobe Photoshop 7.0). Fourier transform infrared (FT-IR) spectra were recorded using a Nicolet170-SX instrument (Thermo Nicolet Ltd., USA) in the wavenumber range of 4000–400 cm^{-1}. The surface elemental composition of the samples was identified by X-ray photoelectron spectroscopy (XPS) using an axis ultra DLD apparatus (Kratos, U.K.). Small-angle X-ray diffraction (SAXRD) was carried out using a diffractmeter type D/max-rA (Rigaku Co., Japan) with Cu target and Ka radiation (λ = 0.154 nm). ζ-Potential analysis was preformed using a Nano-25 zetasizer (Malven, England).

2.6. Inhibition of bacterial activity

The method used for studying the bacterial inhibition activity of nanofibrous mats was reported previously (Son, Yeom, Song, Lee, & Hwang, 2009). Gram-negative *E. coli* was selected as representative microorganism and cultivated in culture medium in an incubator. The nanofibrous mats were sterilized under an ultraviolet radiation lamp for 30 min and then cut in squares of 1 cm × 1 cm, loaded in 2 mL bacterial culture medium, and finally incubated at 37 °C for 18 h. Based on the optical density (OD) in the UV–vis measurement (Shanghai, China), we could evaluate the bacterial inhibition

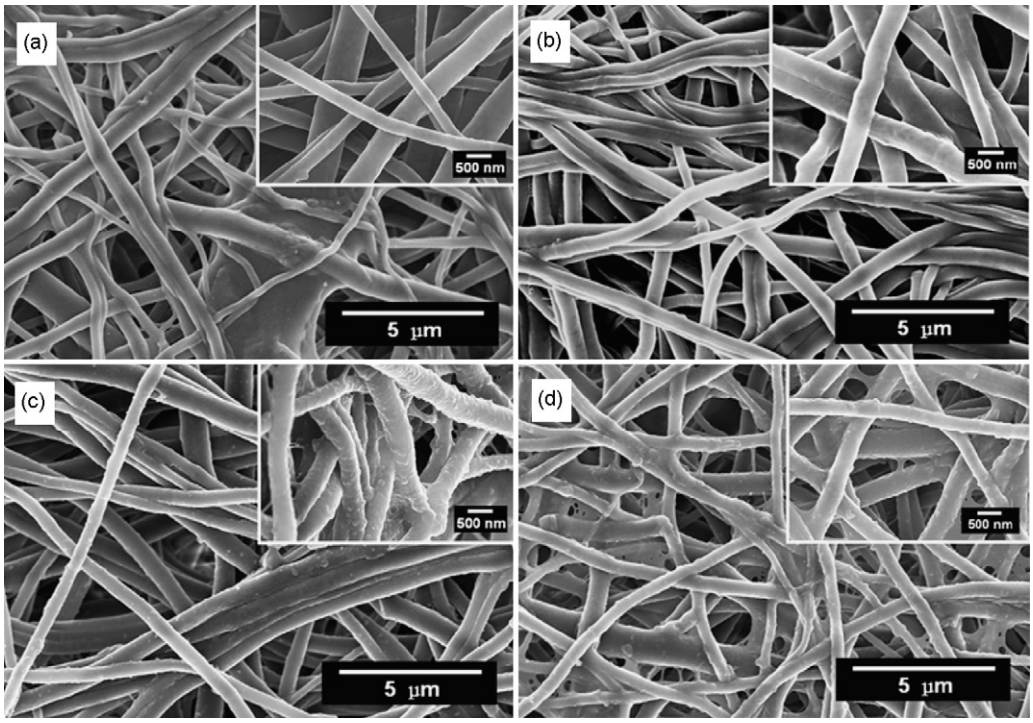

Fig. 1. FE-SEM images of $(CS/ALG)_n$ films coated fibers: (a) $n = 5$, (b) $n = 5.5$, (c) $n = 10$, and (d) $n = 10.5$.

activity from the following equation:

$$\text{Bacterial inhibition activity} = \frac{A - B}{A} \times 100\% \quad (1)$$

where A and B are the number of surviving cells in the control and test samples, respectively.

3. Results and discussion

3.1. Electrospinning and hydrolysis of CA fibrous mats

The typically electrospun nanofibrous mats have a 3D structure with pores in micro- and sub-micro- size (Ding, Fujimoto, & Shiratori, 2005). The FE-SEM images of CA mats and hydrolyzed CA mats were reported in our previous report (Deng et al., 2010). The CA mats contained loosely packed fibers with average fiber diameter of 370 ± 125 nm. After alkaline hydrolysis, the fiber diameter (401 ± 126 nm) was remarkably enlarged compared to CA fibers. The composition of hydrolyzed CA mats was verified by FT-IR, which showed that the pure cellulose nanofibers were obtained after the alkaline hydrolysis process (Deng et al., 2010).

3.2. CS/ALG multilayer modified cellulose nanofibrous mats

In order to investigate the effects of different deposition conditions such as the number of coating bilayers and the composition of the outermost layer on the formation of LBL film-coated fibrous mats, a series of LBL structured polysaccharide films were deposited on cellulose nanofibers. The morphology of the samples is shown in Fig. 1 and the characteristic of the samples is shown in Table 1. There was no obvious difference in morphology between 5 and 5.5 bilayers coated mats, as well as 10 and 10.5 bilayers coated mats (Deng et al., 2010). However, doubling the bilayers showed thicker deposition, more bundles, and bigger junctions as observed from FE-SEM images (Deng et al., 2010). The average thickness of LBL films increased with increasing number of coating films (Table 1). It can be concluded that the number of coating bilayers played an important role in the formation and morphology of LBL film-coated fibrous mats.

Additionally, the surface of LBL structured films coated samples with irregular protuberances are much rougher than that of the cellulose fibers, which could be attributed to the inhomogenous LBL films deposition (Deng et al., 2010). The more bilayers coated, the more protuberances observed. Different from other flat templates, the deposition space among the adjacent fibers in nanofibrous mats is limited and different from each other, which could result in the imbalance of the deposition driven force among the fibers. The dispersion speed of deposition materials into cellulose mats was different as nanofibers distributed in the various sites (Ding, Li, Fujita et al., 2006), so the deposition materials conglomerated with isostatically anomaly. Therefore, the surface layers were enriched

Table 1
The characteristics of LBL films coated cellulose nanofibrous mats.

Samples	Average fiber diameter (nm)	Standard deviation (nm)	Average film thickness (nm)	Average bilayer thickness (nm)
Cellulose-$(CS/ALG)_5$	479	163	78	16
Cellulose-$(CS/ALG)_{5.5}$	459	138	58	11
Cellulose-$(CS/ALG)_{10}$	486	147	85	9
Cellulose-$(CS/ALG)_{10.5}$	485	183	84	8
Cellulose-$(CS\text{-}OREC/ALG)_5$	530	192	129	26
Cellulose-$(CS\text{-}OREC/ALG)_{5.5}$	500	156	99	18
Cellulose-$(CS\text{-}OREC/ALG)_{10}$	640	185	239	24
Cellulose-$(CS\text{-}OREC/ALG)_{10.5}$	523	179	122	12

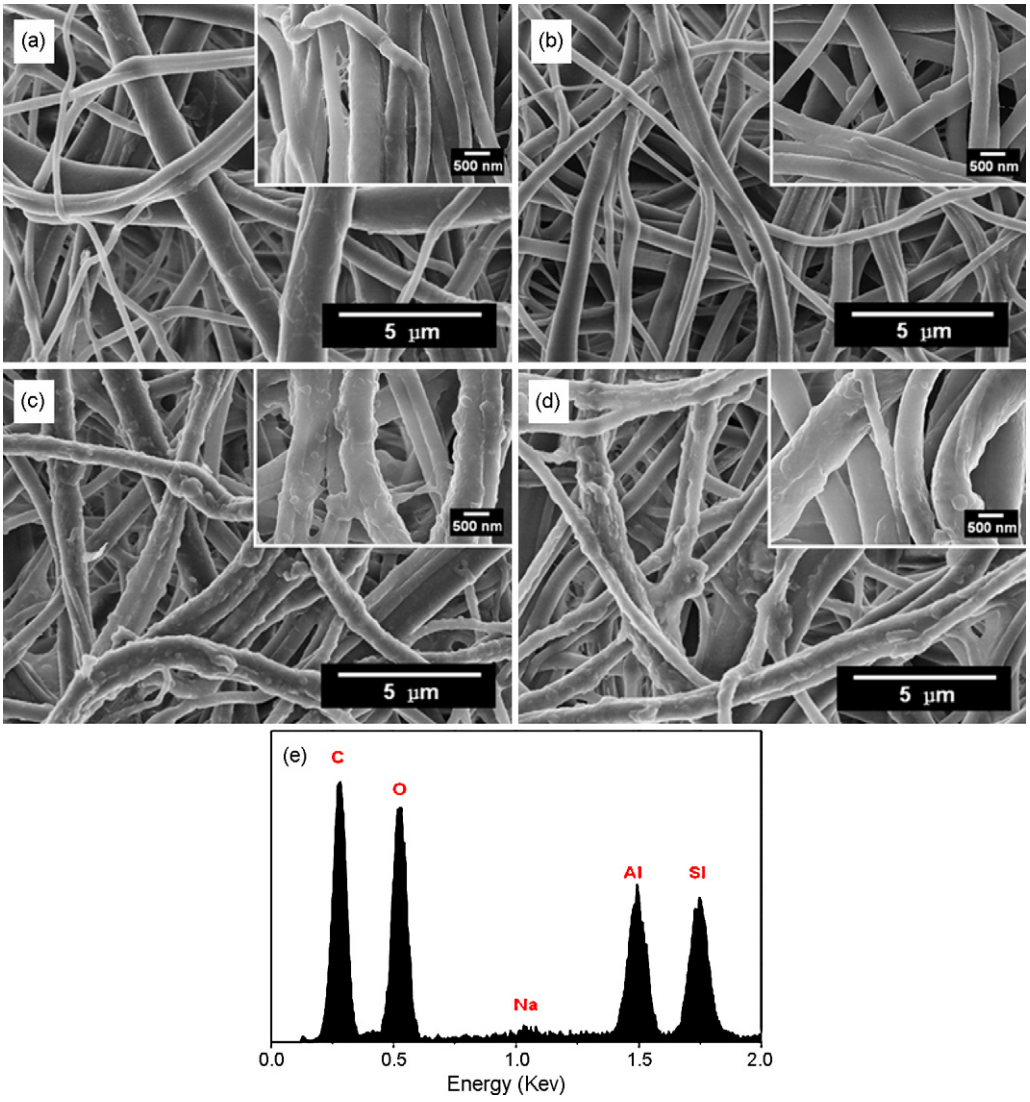

Fig. 2. FE-SEM images of $(CS\text{-}OREC/ALG)_n$ films coated fibers: (a) $n = 5$, (b) $n = 5.5$, (c) $n = 10$, (d) $n = 10.5$ and (e) EDX spectrum of selected $(CS\text{-}OREC/ALG)_{10.5}$ films coated fibers.

in segments from the outermost layer. When the next layer was deposited, it would interpenetrate into the previously adsorbed layer at the same time (Shiratori & Rubner, 2000).

3.3. OREC-containing polysaccharide modified nanofibrous mats

Intercalated CS-OREC solution was introduced as deposition materials to modify the cellulose nanofibers. Fig. 2 shows the FE-SEM images of nanofibrous cellulose mats coated with 5, 5.5, 10, and 10.5 CS-OREC/ALG bilayers. All the mats still maintained the nanofibrous 3D structure after LBL deposition. Correspondingly, the diameter varieties in Table 1 were almost identical to that of CS/ALG coating. However, there was remarkable fiber diameter increase when OREC was introduced into the deposition materials. More junctions, denser bundles and much bigger protuberances formed in the resultant mats because of the high positive charge (+26.4 mV) of CS-OREC composite. In Table 2, the CS and CS-OREC composites have ζ-potential value of +25.5 and +26.4 mV, respectively. The intercalated CS-OREC composite with higher positive charge and larger specific surface area could adsorb more ALG through electrostatic interactions. Thus, in the first step of LBL process, more and thicker CS-OREC could be assembled on cellulose fibers than CS itself, which would adsorb more ALG in the next step. Therefore, LBL films containing OREC was thicker than that of films without OREC. As a result, the morphology of LBL films coated mats was greatly affected by the introduction of OREC. EDX spectrum was recorded to identify the expected compositions on a selected rectangle area of $(CS\text{-}OREC/ALG)_{10.5}$ film-coated nanofibrous mats (Fig. 2e). The characteristic peaks of Si, Al, and Na elements in the spectrum were undentified. As we know, the main components of OREC include Si, Al, and Na elements. The EDX result indicated that OREC was successfully coated on the cellulose nanofibrous mats.

XPS scans were used to further verify the surface compositions of resultant samples. Fig. 3 shows the XPS narrow scan results of $(CS\text{-}OREC/ALG)_n$ film-coated mats. The surface layer of $(CS\text{-}OREC/ALG)_{10.5}$ films coated mats showed peaks characteristic of Si (Si 2p, Fig. 3a) and Al (Al 2p, Fig. 3b), which was identical to the results of EDX. Additionally, a nitrogen peak (N 1s) around 400 eV was detected in all samples (Fig. 3c–f). The XPS results together with

Table 2
ζ-Potential (mV) of REC, OREC, CS, ALG, cellulose nanofibrous mats, and CS-OREC intercalated composites (12/1).

Samples	REC	OREC	CS	ALG	Cellulose	CS-OREC
ζ-Potential (mV)	−7.43	−9.35	25.5	−55.1	−21.3	26.4

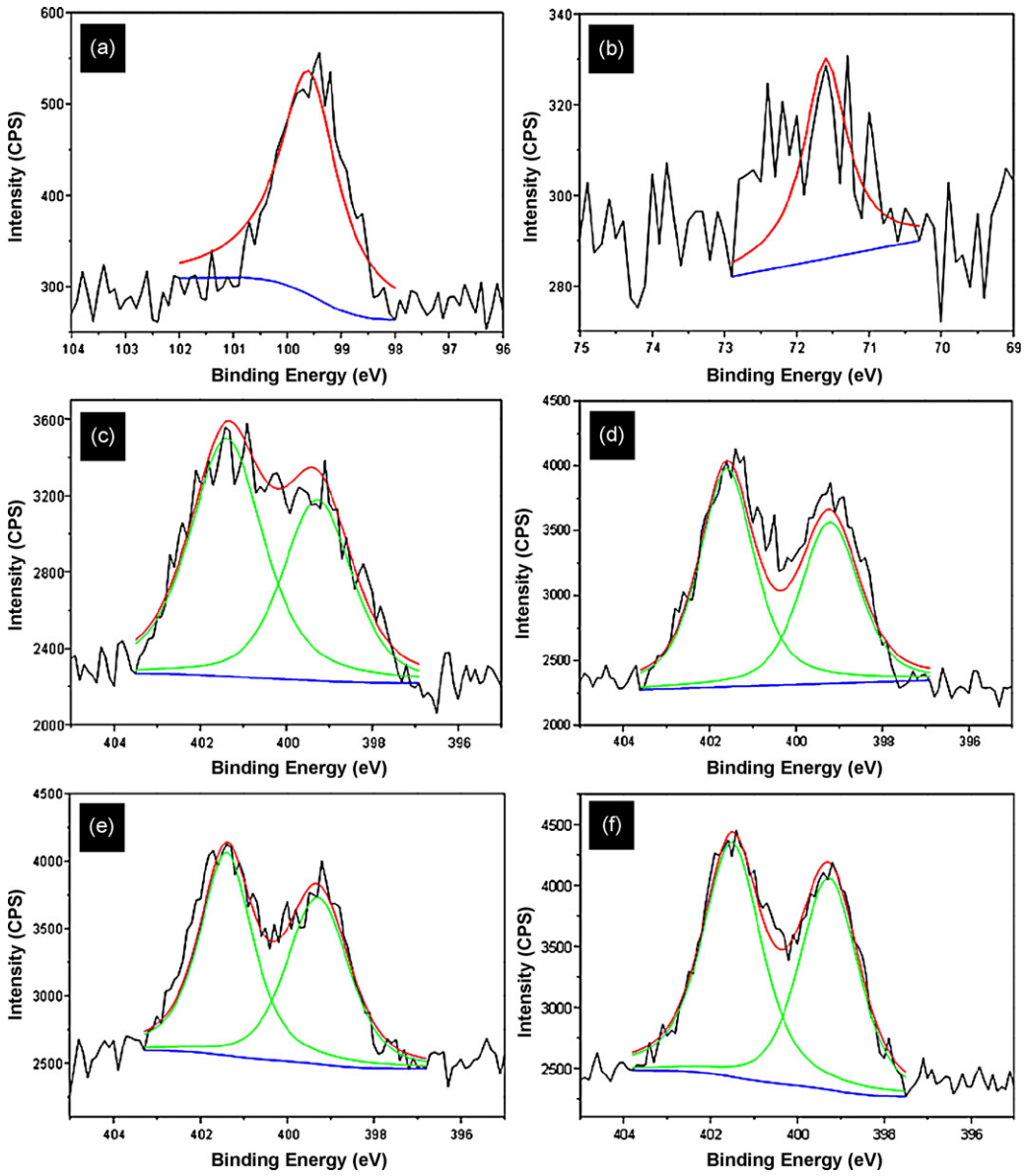

Fig. 3. XPS narrow scans with the curve fit of $(CS\text{-}OREC/ALG)_n$ films coated fibers: Si 2p (a) and Al 2p (b) while $n = 10.5$, and for N 1s scans $n = 5$ (c), $n = 5.5$ (d), $n = 10$ (e), and $n = 10.5$ (f).

the above EDX spectrum proved that CS and OREC were successfully coated on the cellulose fibers. Fig. 3c–f shows the XPS survey scans of the samples with different numbers of CS-OREC/ALG bilayers. The intensity of N 1s peak increased concomitantly with the number of bilayers deposited. N 1s peak in the XPS spectra increased from 3.159 to 4.629 at.% as the number of bilayers increased from 5 to 10.5 (Table 3), indicating that the assembly of different numbers of bilayers onto the cellulose nanofibrous mats was successful. N 1 s peak shows two significant peaks (Fig. 3c–f) for the curve fit at 401.4 eV (protonated amine) and 399.4 eV (amine) (Lawrie et al., 2007). When CS-OREC was the outermost layer (5.5 and 10.5 bilayers) of LBL structured samples, the amine groups extending in dipping solutions became deprotonated when they were washed in neutral rinsing baths and dried in vacuum. When ALG is the outermost layer, the amine groups of the underlying CS-OREC layer will be protonated to a larger degree because of their interaction with deprotonated carboxylate groups of ALG (Lawrie et al., 2007). We speculated that the LBL film coated mats contain a higher amount of protonated amines when ALG is the outermost layer. The atomic percent of the N 1s peak corresponding to the protonated amine (at 401.4 eV) was ranged from 55.5 to 60.1%. The higher atomic percentage of N 1s can be obtained when ALG was the outermost layer (Lawrie et al., 2007).

Table 3
XPS N 1s narrow scan results for different number of $(CS\text{-}OREC/ALG)_n$ bilayers on cellulose mats (the atomic percent of various nitrogen species was determined by curve fitting to the N 1s peak in the XPS spectra).

Samples	N 1s (at.%)	N 1s (protonated amine) (at.%)
Cellulose-$(CS\text{-}OREC/ALG)_5$	3.195	56.944
Cellulose-$(CS\text{-}OREC/ALG)_{5.5}$	3.457	55.569
Cellulose-$(CS\text{-}OREC/ALG)_{10}$	3.939	60.145
Cellulose-$(CS\text{-}OREC/ALG)_{10.5}$	4.629	58.203

To investigate the building of predesigned intercalated architecture in LBL films, the SAXRD patterns of fibrous samples were recorded. Fig. 4a–c and e shows indistinguishable peaks for CS, ALG, cellulose and CS/ALG films coated fibers. Fig. 4d shows the corresponding azimuthally averaged radial intensity trace. The maximum intensity is located at $2\theta = 2.40^\circ$, which corresponds to

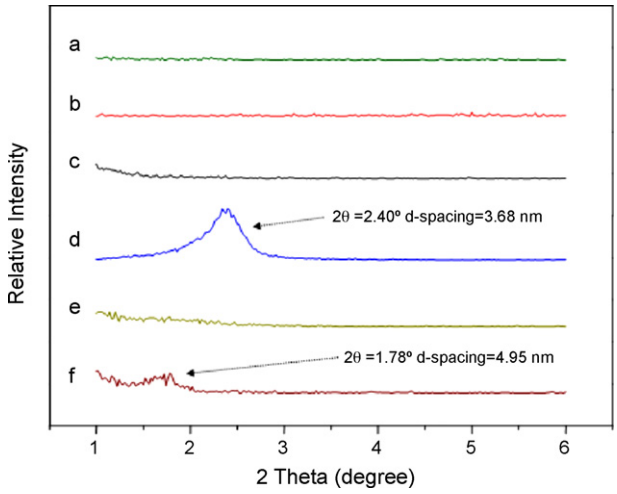

Fig. 4. SAXRD patterns of (a) CS powder, (b) ALG powder, (c) cellulose nanofibrous mats, (d) OREC powder, (e) $(CS/ALG)_{10.5}$ films coated fibers, and (f) $(CS\text{-}OREC/ALG)_{10.5}$ films coated fibers.

a mean correlation distance between the interlayers of OREC of 3.68 nm, as calculated by Bragg's equation:

$$2d \sin \theta = n\lambda \quad (2)$$

where d is the interlayer spacing, θ is the angle of incidence, λ is wave length, and n is an integer, the order of the reflection. In Fig. 4e, there was no obvious SAXRD curve for $(CS/ALG)_{10.5}$ films coated mats. Fig. 4f shows the SAXRD pattern of $(CS\text{-}OREC/ALG)_{10.5}$ films deposited mats. The spacing distance between OREC interlayers enlarged to 4.95 nm. In comparison with OREC, the SAXRD curves of $(CS\text{-}OREC/ALG)_{10.5}$ films coated nanofibrous mats diminished, which confirmed that CS was intercalated to the interlayers of OREC. This result was consistent with our previous report (Wang et al., 2006).

3.4. Bacterial inhibition activity

The degree of bacteria growth inhibition for *E. coli* was examined in LBL structured samples with different surface compositions and coating bilayers. The concentrations of microorganism suspension were 10^5 and 10^7 CFU/mL. It was found in Fig. 5 that all the LBL films coated nanofibrous mats had bacterial inhibition activity because of the presence of CS. Fig. 5A shows the bacterial inhibition activity of the samples with lower microorganism concentration (10^5 CFU/mL). The growth inhibition of $(CS\text{-}OREC/ALG)_{10.5}$ films coated nanofibrous mats was 73%, while the growth inhibition of CS/ALG film-coated mats was less than 45%. The growth inhibition of LBL films coated mats with CS in the outermost layer was around 45%, while the growth inhibition of the samples with ALG in the outermost layer was lower than 30%. The results indicated that the addition of OREC improved the antibacterial activity of the nanofibrous mats, and the antimicrobial activity of the samples with CS in the outermost layer was better than that of the samples with ALG in the outermost layer. The similar result was found in the samples treated with 10^7 CFU/mL *E. coli* (Fig. 5B). LBL films coated nanofibrous mats had a little bacterial inhibition ability at high microorganism concentration. The bacterial inhibition of $(CS\text{-}OREC/ALG)_{10.5}$ coated mats was higher than that of CS/ALG coated fibrous mats. The mats with CS in the outermost layer had better bacterial inhibition activity than the mats with ALG in the outermost layer. The increase of bacterial inhibition with the addition of OREC may be caused by three reasons (Wang et al., 2006): first, the bacterial adsorption and immobilization capacities of CS-OREC were increased because of its hydrophobicity and higher positive charge; second, CS has antimicrobial activity; third, the bigger protuberances contained nanofibrous mats that have higher surface area to volume ratio, which may cause efficient contact and interaction with bacterial.

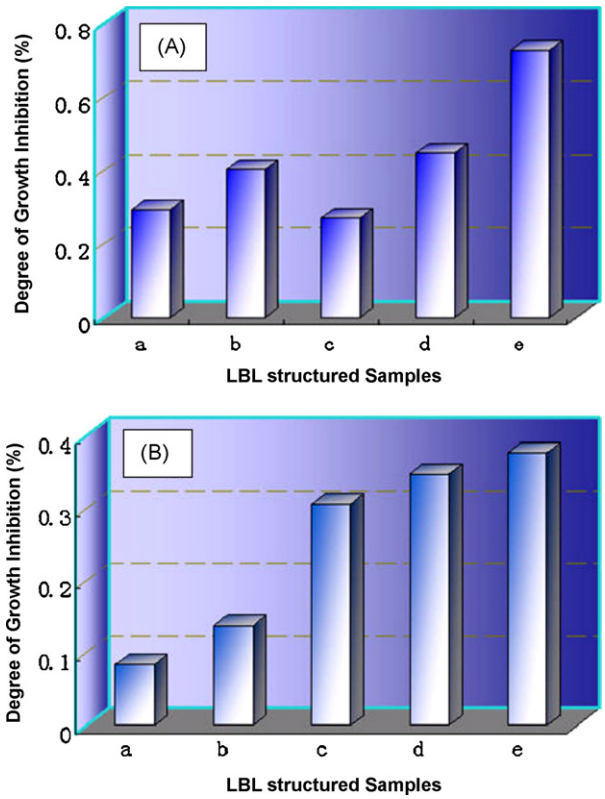

Fig. 5. (A) degree of growth inhibition of (a) $(CS/ALG)_5$, (b) $(CS/ALG)_{5.5}$, (c) $(CS/ALG)_{10}$, (d) $(CS/ALG)_{10.5}$, and (e) $(CS\text{-}OREC/ALG)_{10.5}$ films coated nanofibrous mats on 10^5 CFU/mL *E. coli*. (B) Degree of growth inhibition of (a) $(CS/ALG)_5$, (b) $(CS/ALG)_{5.5}$, (c) $(CS/ALG)_{10}$, (d) $(CS/ALG)_{10.5}$, and (e) $(CS\text{-}OREC/ALG)_{10.5}$ films coated nanofibrous mats on 10^7 CFU/mL *E. coli*.

4. Conclusions

LBL films modified nanofibrous cellulose mats with antibacterial property were successfully fabricated from the oppositely charged CS-OREC intercalation solution and the negatively charged ALG solution via LBL self-assembly technique. The morphology of LBL films coated nanofibrous cellulose mats was greatly influenced by deposition conditions. The resultant samples still maintained prefect fiber shape and 3D structure. The EDX and XPS results demonstrated that OREC and CS were assembled on the surface of the fibers. The SAXRD data showed that OREC was intercalated by CS and the interlayer distance of OREC was enlarged by CS chains. The introduction of OREC to LBL films led to thicker bilayer and better antibacterial activity. Furthermore, the developed approach to immobilize layered silicate onto polymer nanofibers with controllable thickness and enlarged interlayer distance may also be utilized to tailor the sizes, compositions, and surface properties of other 3D LBL structured materials with tunable ζ-potential value for various applications such as catalysis, sensors, tissue engineering, and antimicrobial wound dressing.

Acknowledgments

This project was funded by the State Key Laboratory for Modification of Chemical Fibers and Polymer Materials, Donghua University, China. Partial support from the Program of Introducing

Talents of Discipline to Universities (No. 111-2-04 and B07024) and the National Natural Science Foundation of China (No. 30972323) were appreciated.

References

Darder, M., Colilla, M., & Ruiz-Hitzky, E. (2003). Biopolymer-clay nanocomposites based on chitosan intercalated in montmorillonite. *Chemistry of Materials*, *15*, 3774–3780.

Decher, G. (1997). Fuzzy nanoassemblies: Toward layered polymeric multicomposites. *Science*, *277*, 1232–1237.

Decher, G., & Hong, J. D. (1991). Buildup of ultra-thin multilayer films by a self-assembly process: II. Consecutive Adsorption of Anionic and Cationic Bipolar Amphiphiles and Polyelectrolytes on Charged Surfaces. *Berichte Der Bunsengesellschaft Fur Physikalische Chemie*, *95*, 1430–1434.

Deng, H. B., Zhou, X., Wang, X. Y., Zhang, C. Y., Ding, B., Zhang, Q. H., et al. (2010). Layer-by-layer structured polysaccharides film-coated cellulose nanofibrous mats for cell culture. *Carbohydrate Polymers*, *80*, 474–479.

Ding, B., Fujimoto, K., & Shiratori, S. (2005). Preparation and characterization of self-assembled polyelectrolyte multilayered films on electrospun nanofibers. *Thin Solid Films*, *491*, 23–28.

Ding, B., Kimura, E., Sato, T., Fujita, S., & Shiratori, S. (2004). Fabrication of blend biodegradable nanofibrous nonwoven mats via multi-jet electrospinning. *Polymer*, *45*, 1895–1902.

Ding, B., Li, C. R., Fujita, S., & Shiratori, S. (2006). Layer-by-layer self-assembled tubular films containing polyoxometalate on electrospun nanotibers. *Colloids and Surfaces: A-Physicochemical and Engineering Aspects*, *284*, 257–262.

Ding, B., Li, C. R., Miyauchi, Y., Kuwaki, O., & Shiratori, S. (2006). Formation of novel 2D polymer nanowebs via electrospinning. *Nanotechnology*, *17*, 3685–3691.

Elbakry, A., Zaky, A., Liebkl, R., Rachel, R., Goepferich, A., & Breunig, M. (2009). Layer-by-layer assembled gold nanoparticles for siRNA delivery. *Nano Letters*, *9*, 2059–2064.

Giannelis, E. P., Krishnamoorti, R., & Manias, E. (1999). Polymer-silicate nanocomposites: Model systems for confined polymers and polymer brushes. *Polymers in Confined Environments*, *138*, 107–147.

Ingrosso, C., Petrella, A., Curri, M. L., Striccoli, M., Cosma, P., Cozzoli, P. D., et al. (2006). Photoelectrochemical properties of hybrid junctions based on zinc phthalocyanine and semiconducting colloidal nanocrystals. *Electrochimica Acta*, *51*, 5120–5124.

Ji, Y., Ghosh, K., Shu, X. Z., Li, B. Q., Sokolov, J. C., Prestwich, G. D., et al. (2006). Electrospun three-dimensional hyaluronic acid nanofibrous scaffolds. *Biomaterials*, *27*, 3782–3792.

Kim, J. S., Rieter, W. J., Taylor, K. M. L., An, H., Lin, W. L., & Lin, W. B. (2007). Self-assembled hybrid nanoparticles for cancer-specific multimodal imaging. *Journal of the American Chemical Society*, *129*, 8962–8963.

Lawrie, G., Keen, I., Drew, B., Chandler-Temple, A., Rintoul, L., Fredericks, P., et al. (2007). Interactions between alginate and chitosan biopolymers characterized using FTIR and XPS. *Biomacromolecules*, *8*, 2533–2541.

Lee, S. W., Kim, B. S., Chen, S., Shao-Horn, Y., & Hammond, P. T. (2009). Layer-by-layer Assembly of All carbon nanotube ultra-thin films for electrochemical applications. *Journal of the American Chemical Society*, *131*, 671–679.

Liu, H. Q., & Hsieh, Y. L. (2002). Ultrafine fibrous cellulose membranes from electrospinning of cellulose acetate. *Journal of Polymer Science Part B-Polymer Physics*, *40*, 2119–2129.

Shahidi, F., Arachchi, J. K. V., & Jeon, Y. J. (1999). Food applications of chitin and chitosans. *Trends in Food Science & Technology*, *10*, 37–51.

Shiratori, S. S., & Rubner, M. F. (2000). pH-dependent thickness behavior of sequentially adsorbed layers of weak polyelectrolytes. *Macromolecules*, *33*, 4213–4219.

Son, B., Yeom, B. Y., Song, S. H., Lee, C. S., & Hwang, T. S. (2009). Antibacterial electrospun chitosan/poly(vinyl alcohol) nanofibers containing silver nitrate and titanium dioxide. *Journal of Applied Polymer Science*, *111*, 2892–2899.

Srivastava, S., & Kotov, N. A. (2008). Composite layer-by-layer (LBL) assembly with inorganic nanoparticles and nanowires. *Accounts of Chemical Research*, *41*, 1831–1841.

Unal, U., Ida, S., Shimogawa, K., Altuntasoglu, O., Izawa, K., Ogata, C., et al. (2006). Electrochemical behavior of Ag+ intercalated layered oxides. *Journal of Electroanalytical Chemistry*, *595*, 95–102.

Wang, X. Y., Du, Y. M., Luo, J. W., Yang, J. H., Wang, W. P., & Kennedy, J. F. (2009). A novel biopolymer/rectorite nanocomposite with antimicrobial activity. *Carbohydrate Polymers*, *77*, 449–456.

Wang, X. Y., Du, Y. M., Yang, H. H., Wang, X. H., Shi, X. W., & Hu, Y. (2006). Preparation, characterization and antimicrobial activity of chitosan/layered silicate nanocomposites. *Polymer*, *47*, 6738–6744.

Wang, X. Y., Pei, X. F., Du, Y. M., & Li, Y. (2008). Quaternized chitosan/rectorite intercalative materials for a gene delivery system. *Nanotechnology*, *19*, 65706.

Wang, S. H., Shi, X. Y., Chen, X. S., & Baker, J. R. (2009). Therapeutic efficacy of 2-methoxyestradiol microcrystals encapsulated within polyelectrolyte multilayers. *Macromolecular Bioscience*, *9*, 429–436.

Wang, X. Y., Strand, S. P., Du, Y. M., & Varum, K. M. (2010). Chitosan-DNA-rectorite nanocomposites: Effect of chitosan chain length and glycosylation. *Carbohydrate Polymers*, *79*, 590–596.

Xiao, S. L., Wu, S. Q., Shen, M. W., Guo, R., Huang, Q. G., Wang, S. Y., et al. (2009). Polyelectrolyte multilayer-assisted immobilization of zero-valent iron nanoparticles onto polymer nanofibers for potential environmental applications. *Acs Applied Materials & Interfaces*, *1*, 2848–2855.

Yang, A., Tao, X. M., Pang, G. K. H., & Siu, K. G. G. (2008). Preparation of porous tin oxide nanobelts using the electrospinning technique. *Journal of the American Ceramic Society*, *91*, 257–262.

Zhang, L. B., Chen, H., Sun, J. Q., & Shen, J. C. (2007). Layer-by-layer deposition of poly(diallyldimethylammonium chloride) and sodium silicate multilayers on silica-sphere-coated substrate-facile method to prepare a superhydrophobic surface. *Chemistry of Materials*, *19*, 948–953.